

Lossless Direct Path Reinforced Bidirectional DC-DC Converter for On-Board Charger in Electric Vehicle

Veeramani Veerakgoundar¹, Senthilkumar Subramaniam¹,
Sowthily Chandrasekharan¹

Abstract: A DC-DC converter plays a vital role in the On-Board Charger for Electric Vehicles (EVs). Also, having the capability for bidirectional power flow for a DC-DC converter is essential for EVs to transfer power from Vehicle-to-Grid (V2G) and Vehicle-to-Vehicle (V2V). In this context, this paper proposes a bidirectional DC-DC converter for the On-Board Charger for Electric Vehicles (EVs). The proposed DC-DC converter has two paths: a lossy partial path through two bridges, a high-frequency transformer, and a lossless direct path directly connecting the source to the output. A 7.8 kW DC-DC converter is developed in MATLAB/Simulink. The performance of the converter is analysed for various operating scenarios. Further, a scaled-down hardware prototype of the proposed converter with a power rating of 600 W has been developed. The dSPACE controller is used to control the power flows. The prototype is tested under various operating conditions. The experimental and simulation results show that the power flow through the direct path is around 58 % and through the partial path around 42 %. Due to this, the overall converter efficiency of 97.8% during charging and 95.6 % during discharging cycles has been achieved. Also, as only 42 % of power flows through the partial path, all the components' ratings and sizes are significantly reduced. Also, the distinguishing feature is its bidirectional power flow capability, making the EV capable of V2V and V2G power transfer. Hence, the proposed DC-DC converter is an efficient and compact solution for an On-Board Charger for EVs.

Keywords: Constant Current Charging, Electric Vehicle, High Frequency Transformer (HFT), On-Board Charger (OBC), Vehicle-to-Vehicle(V2V), Vehicle-to-Grid(V2G).

1 Introduction

In recent years, Electrical Vehicles (EVs) are fast replacing conventional petrol or diesel-driven vehicles to substantially reduce air pollution and global

¹Department of Electrical and Electronics Engineering, National Institute of Technology, Tiruchirappalli, India, PIN – 620 015; E-mails: vveeramani86@gmail.com; skumar@nitt.edu; sowthilyc@gmail.com

warming and overcome the issue of fast-depleting fossil fuels [1]. Nowadays, EVs are used for neighbourhood applications with a battery pack of 36V-72V range [2], light EVs with 300V- 420V, and heavy EVs up to 800V [3]. Unlike the situation at the beginning of rolling out EVs, the charging facilities have now increased substantially, so the travel distance could be much longer. However, EVs' weight and overall cost remain on the higher side [4]. Further, issues like slow charging time, battery life span, charger efficiency, and compactness are to be suitably addressed [5]. From a charger design perspective, EVs are generally classified as On-Board Chargers (OBC) and Off-Board chargers [6, 7]. In EVs with an OBC, the space occupied by the charger is an important constraint. Therefore, designing and developing compact, highly efficient chargers is one of the critical and challenging tasks in On-Board EV applications [8]. OBC generally consist of the following power conversion stages: AC/DC rectification and DC/DC charging. Sometimes, it can include one more DC/DC intermediate stage [9, 10]. In each stage, compactness, higher efficiency, fast charging with industry standards and handling safety policy makes the systems more complex in OBC [11]. Much work has been done to improve the efficiency and power factor of the AC/DC Stage [12, 13]. However, size reduction in this stage is quite challenging due to the need for a high-volume capacitance [14]. In this context, the DC/DC stage of the charger will have a crucial impact on the size and efficiency of the OBC. Hence, many researchers focus on designing and developing DC/DC converters for OBC in EVs.

Recently, many isolated DC-DC converter topologies have been proposed for the DC-DC stage of On-Board EV applications [15]. A resonant type of isolated converter design for EV applications is proposed in [16] to minimize the switching and conduction losses. However, it has one more DC-DC stage and is bulky. An isolated DC-DC stage of the OBC has been presented to address the short-range Zero Voltage Switching (ZVS), duty cycle losses, and circulating current issues. All these issues are mitigated with additional support from Capacitor-Diode-Diode (CDD) snubber circuits and conventional Phase Shifted Full Bridge Converter (PSFBC) [17]. A full bridge (Inductor-inductor-capacitor) LLC resonant converter was developed for the DC-DC Stage of EVs charger with improved efficiency [18]. However, the performance degrades if the switching frequency is away from resonant points. The isolated topologies in [16 – 18] do not have bidirectional power flow features. In addition, achieving higher power density and efficiency during the charging cycle is challenging.

Nowadays, the OBC of an EV should be capable of using batteries in the vehicle for the following uses in addition to powering the EV: (i) standalone mode for outdoor lighting when needed, (ii) Vehicle to Grid (V2G) at peak demand (iii) Vehicle to Vehicle (V2V) power transfer during emergencies. Bidirectional power flow capability should be a vital feature for the DC-DC converter to be helpful for these applications mentioned [19]. Hugo Neves de Melo *et al.* have

proposed a compact non-isolated DC-DC converter for OBC with a bidirectional power flow feature. However, this method introduces power quality issues on the utility grid side [20]. Several DC-DC isolated bidirectional converter topologies using soft switching features have been described recently [21 – 23]. References [24 – 26] deal with DC-DC converter topologies to reduce the switching losses, DC link ripple issues, and improved voltage transfer ratios for V2V integration. However, these topologies will be affected by magnetic saturation at higher switching frequencies [27]. Above all, the works in [16 – 27] use converters with full power processing topology. Despite the many advantages of this topology, designing a compact charger with high efficiency remains challenging.

In the 1990s, the partial power processing concept was introduced by the *National Aeronautics and Space Administration* (NASA) to make a compact and efficient Series Connected Boost Unit (SCBU) for aircraft applications [28]. Recently a fast EV charging station has been developed using this concept [29]. However, this topology cannot provide galvanic isolation and cannot be used in V2G applications. Moreover, duty cycle loss and circulating currents are other drawbacks. Bhaskar *et al.* surveyed various non-isolated unidirectional electrical vehicle charger topologies [30]. Non-isolation is usually thought of as a safety concern. However, as per the safety standards such as the Society of Automotive Engineers (SAE) SAEJ1772 and Automotive Industry Standard (AIS) AIS-138, galvanic isolation is not required for OBC applications owing to the reason that the battery will be floating with the body ground [31 – 33].

In this context, this paper proposes a novel non-isolated bidirectional DC-DC converter for an On-Board Charger for EVs. The power flows in both directions via two paths: one directly connected to the output and the other through the bridge network. The performance of the proposed converter is analysed by developing a MATLAB/Simulink model with a power rating of 7.8 kW and validating it for various operating scenarios. Further, the scaled-down 600 W hardware setup is built, and dSPACE is used to control the power flows. The source voltage is 30 V DC, and the load is 48 V/12.5 Ah battery. The developed hardware is tested for different operating scenarios, and the performance is validated. The proposed DC-DC converter achieves an overall efficiency of 97% with fewer components compared to other works in the literature. The main contribution of this work is summarised as follows:

- The proposed DC-DC converter uses a lossless direct path in addition to the partial path comprising the bridges and transformer. At least 55% of the power flows through this lossless direct path during charging and discharging, so a highly efficient power transfer is achieved.
- The power flow through the lossy partial path is less than 45% during both charging and discharging, so the rating and size of the bridge elements and

transformer are significantly reduced. Hence, the overall size and weight of the On-Board Charger can be significantly reduced.

- The bidirectional capability can make the EV capable of V2G and V2V power transfer, a desirable feature for modern EVs.

The performance of the proposed DC-DC converter topology is compared with the recent works and found to offer a high efficiency by using fewer components and being capable of bidirectional power flow.

2 DC-DC Converter in On-Board EV Charger

Generally, the charger for an electric vehicle can be On-Board or Off-Board. An On-Board charger is more flexible than an Off-Board charger, making it the most sought-after charger type for EVs. The typical structure of an On-Board Charger in an EV is shown in Fig. 1. The overall working of the On-Board Charger is as follows. The OBC will be connected to any AC outlet at home, charging stations, parking areas, or workplace. The AC-DC converter rectifies the AC supply to DC and, in addition, does the power factor correction. The DC-DC converter regulates the DC voltage obtained from the AC-DC converter to ensure that it is compatible and controllable while charging the battery.

In the complete structure of the OBC, the DC-DC converter is directly interfaced with the battery. Hence, the fastness of charging, the battery's life span, and the charging efficiency will be significantly influenced by the topology and the power processing technique adopted by the DC-DC converter. In addition, if the EV wants to pump power back to the grid in V2G applications or pump it to other EVs in V2V applications, the DC-DC converter should be capable of a bidirectional power flow feature.

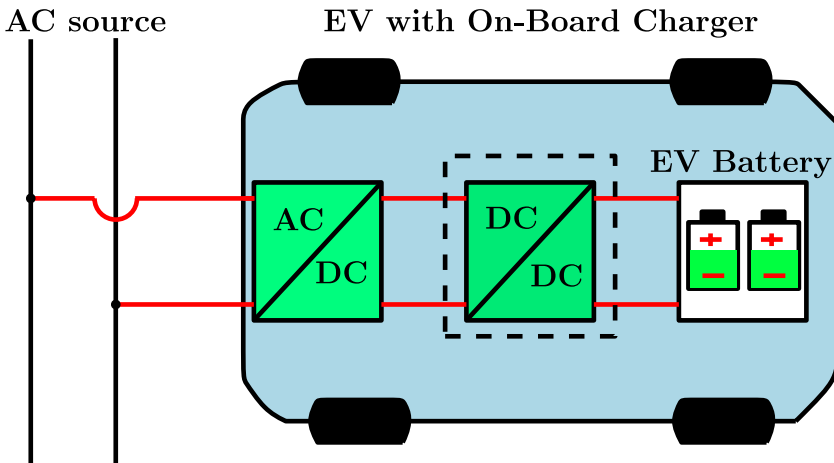


Fig. 1 – Structure of On-Board Charger in EV.

Hence, an efficient and compact bidirectional DC-DC converter will help improve the overall performance of the OBC and the EV and make it capable of participating in V2G and V2V applications. Such a robust DC-DC converter is proposed in the next section.

3 Proposed DC-DC Converter for On-Board Charger

The block diagram of the proposed DC-DC converter and the control strategy is shown in Fig. 2. The proposed converter consists of two MOSFET-based active bridges, a High-Frequency Transformer (HFT), an inductor, and DC filter capacitors. The DC source is fed to the input of the source side MOSFET bridge and feed-forward to the output of the battery side MOSFET bridge. The converter is designed so that the power flow can be bidirectional. During charging, the power flows from the source to the battery via two paths. One path is through the bridges, called the partial power path, and the other is directly from the source, called the direct power path. During discharge, the power flows from the battery to the source via the same partial and direct paths. The power flow during charging and discharging is controlled by the Gate Signals issued by the Single-Phase-Shift Controller (SPSC).

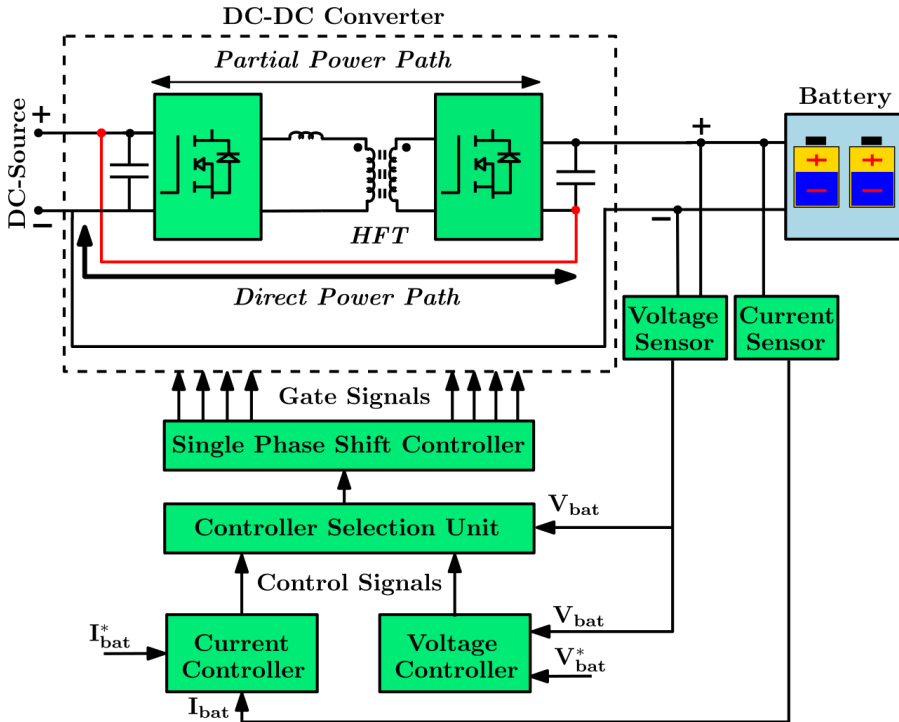


Fig. 2 – Block diagram of the proposed DC-DC converter along with control strategy.

Mode I: $0 < t < t_2$

This mode starts with turning OFF the Q₂-Q₃ pair and turning ON the Q₁-Q₄. The Q₆-Q₇ pair continue in the ON state from the previous mode. The current flow through the inductor prior to this mode was through Q₂-Q₃. On turning ON the Q₁-Q₄, the inductor current starts freewheeling through the body diodes of Q₁ and Q₄ until the current reaches zero, as shown in Fig. 4g. After the freewheeling action, the MOSFETs Q₁-Q₄ start conduction, and the current through the inductor reverses and rises gradually, as shown in Fig. 4g. Hence, the total switching interval of this mode can be divided into two intervals, 0 to t_1 (freewheeling interval) and t_1 to t_2 (conduction interval). The state of the switch during these intervals is shown in Figs. 4a and Fig. 4b. Equation (1) gives the slope of the inductor current.

$$\frac{di_L}{dt} = \frac{V_{dc} - n(V_{dc} - V_{bat})}{L_{ext}}. \quad (1)$$

From (1) we can infer that the slope of the inductor current in this mode will be constant, as the values n , V_{dc} , L_{ext} , and V_{bat} are constant.

Mode II: $t_2 < t < t_3$

The mode starts with the turn ON of Q₅-Q₈ and the turn OFF of Q₆-Q₇. The Q₁-Q₄ pair continues to be in the ON state from Mode I. The state of the switch during this mode is shown in Fig. 4c. The switching action results in a change of the voltage across the inductor. The change in voltage results in the change of slope of the inductor current; thus, the inductor current falls gradually. However, the slope of the inductor current throughout this mode remains constant, as can be understood from (2).

$$\frac{di_L}{dt} = \frac{V_{dc} - n(V_{bat} - V_{dc})}{L_{ext}}. \quad (2)$$

Mode III: $t_3 < t < t_5$

The mode starts with the turn OFF of Q₁-Q₄ and the turn ON of Q₂-Q₃. The Q₅-Q₈ pair continues to be in the ON state from Mode II. In the previous mode, the inductor current was flowing through Q₁-Q₄. On turning ON Q₂-Q₃, the slope of the inductor current changes to negative, and it freewheels through the body diodes of the Q₂-Q₃ pair until it reaches zero, as shown in Fig. 4g. After freewheeling, Q₂-Q₃ starts conduction, and the current through the inductor rises gradually in the reverse direction, as shown in Fig. 4g. The state of the switches during these intervals is shown in Fig. 4d and Fig. 4e. The slope of the inductor current throughout this mode remains constant, as can be understood from (3).

$$\frac{di_L}{dt} = \frac{-V_{dc} - n(V_{bat} - V_{dc})}{L_{ext}}. \quad (3)$$

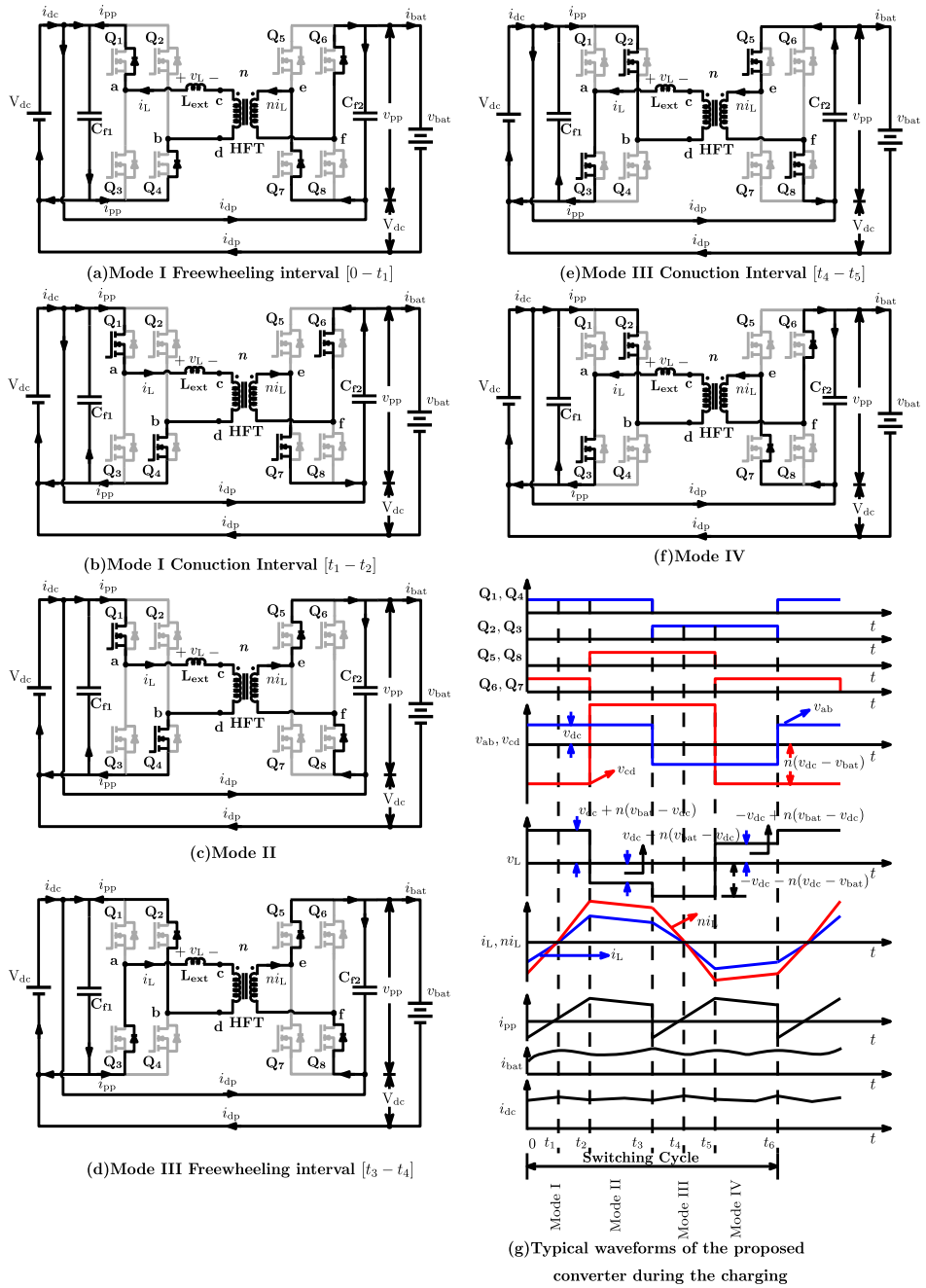


Fig. 4 – Proposed DC-DC converter modes of operation during the charging cycle with typical waveforms.

Mode IV: $t_5 < t < t_6$

This mode starts with the turn ON of Q₆-Q₇ and the turn OFF of Q₅-Q₈. The Q₂-Q₃ pair continues to be in the ON state from Mode III. The state of the switch during this mode is shown in Fig. 4f. The switching action results in a change of the voltage across the inductor. The change in voltage results in the change of slope of the inductor current; thus, the inductor current falls gradually in the reverse direction. However, the slope of the inductor current throughout this mode remains constant, as can be understood from (4).

$$\frac{di_L}{dt} = \frac{-V_{dc} - n(V_{dc} - V_{bat})}{L_{ext}}. \quad (4)$$

3.1.2 Steady-state power flow analysis during charging

The power flow from the source to the battery is analysed for one switching cycle. The average value of the currents and voltages are considered for this analysis. From Fig. 3, the following equations can be arrived.

$$I_{dc} = I_{pp} + I_{dp}, \quad (5)$$

$$V_{bat} = V_{dc} + V_{pp}, \quad (6)$$

where I_{dc} is the DC source current, I_{pp} is the current contributing to the partial path power flow, I_{dp} is the current contributing to the direct path power flow, V_{bat} is the voltage across the battery terminals, V_{dc} is the voltage of the DC source, and V_{pp} is the partial path output voltage.

From Fig. 3, it can be observed that,

$$I_{dp} = I_{bat}. \quad (7)$$

For a particular value of charging current (I_{bat}), the power balance equation can be arrived by multiplying (6) with I_{bat} on both sides, as shown in (8)

$$V_{bat} I_{bat} = V_{dc} I_{bat} + V_{pp} I_{bat}. \quad (8)$$

From (8) it can be inferred that the power delivered to the battery, P_{bat} is contributed by two paths: the component $V_{dc} I_{bat}$ is the power contributed by the direct path P_{dp} , and the component $V_{pp} I_{bat}$ is the power contributed by the partial path, P_{pp-out} . Hence, (8) can be written as

$$P_{bat} = P_{dp} + P_{pp-out}. \quad (9)$$

The overall efficiency of the converter is given by

$$\eta_{charging} = \frac{P_{bat}}{V_{dc} I_{dc}}. \quad (10)$$

Here, the total input power is delivered by the DC source, $P_{dc} = V_{dc} I_{dc}$. Hence, (10) can be written as

$$\eta_{\text{charging}} = \frac{P_{\text{bat}}}{P_{\text{dc}}} = \frac{V_{\text{bat}} I_{\text{bat}}}{V_{\text{dc}} I_{\text{dc}}}. \quad (11)$$

From Fig. 3, the partial path input power, $P_{\text{pp-in}}$ can be defined as

$$P_{\text{pp-in}} = V_{\text{dc}} I_{\text{pp}}. \quad (12)$$

During the charging, power ratios between the partial path and overall charging output power are defined as the partial power-sharing ratio, and it can be expressed as

$$K_{\text{c-ppsr}} = \frac{P_{\text{pp-out}}}{P_{\text{bat}}} = \frac{V_{\text{pp}}}{V_{\text{bat}}} = 1 - \frac{V_{\text{dc}}}{V_{\text{bat}}}. \quad (13)$$

From (8) and (12), the partial path efficiency is calculated as

$$\eta_{\text{c-pp}} = \frac{P_{\text{pp-out}}}{P_{\text{pp-in}}}. \quad (14)$$

Using (9 – 11), (13), and (14), the charging efficiency of the converter was derived and expressed as follows as

$$\eta_{\text{charging}} = 1 - K_{\text{c-ppsr}} (1 - \eta_{\text{c-pp}}). \quad (15)$$

From (15) it can be inferred that the converter's efficiency during charging is influenced by the partial power-sharing ratio ($K_{\text{c-ppsr}}$).

3.1.3 Operation of DC-DC Converter during Discharging Cycle

In this discharging cycle, the power transfer from the battery to the source can be understood by four switching modes of operation of the converter in one complete switching cycle. A unique pair of MOSFETs turn ON in each mode. The voltage of the DC source and the battery does not vary during the switching cycle and is assumed to be constant.

Mode I: $0 < t < t_1$

The mode starts with the turn ON of Q_1 - Q_4 and the turn OFF of Q_2 - Q_3 . The Q_5 - Q_8 pair continues to be in the ON state from the previous mode. The state of the switch during this mode is shown in Fig. 5a. The switching action results in a change of the voltage across the inductor. The change in voltage results in the slope change of the currents i_L and ni_L ; thus, the current ni_L falls gradually. However, the slope of the current ni_L throughout this mode remains constant, as can be understood from (16).

$$\frac{d(ni_L)}{dt} = \frac{V_{\text{dc}} - n(V_{\text{bat}} - V_{\text{dc}})}{L_{\text{ext}}}. \quad (16)$$

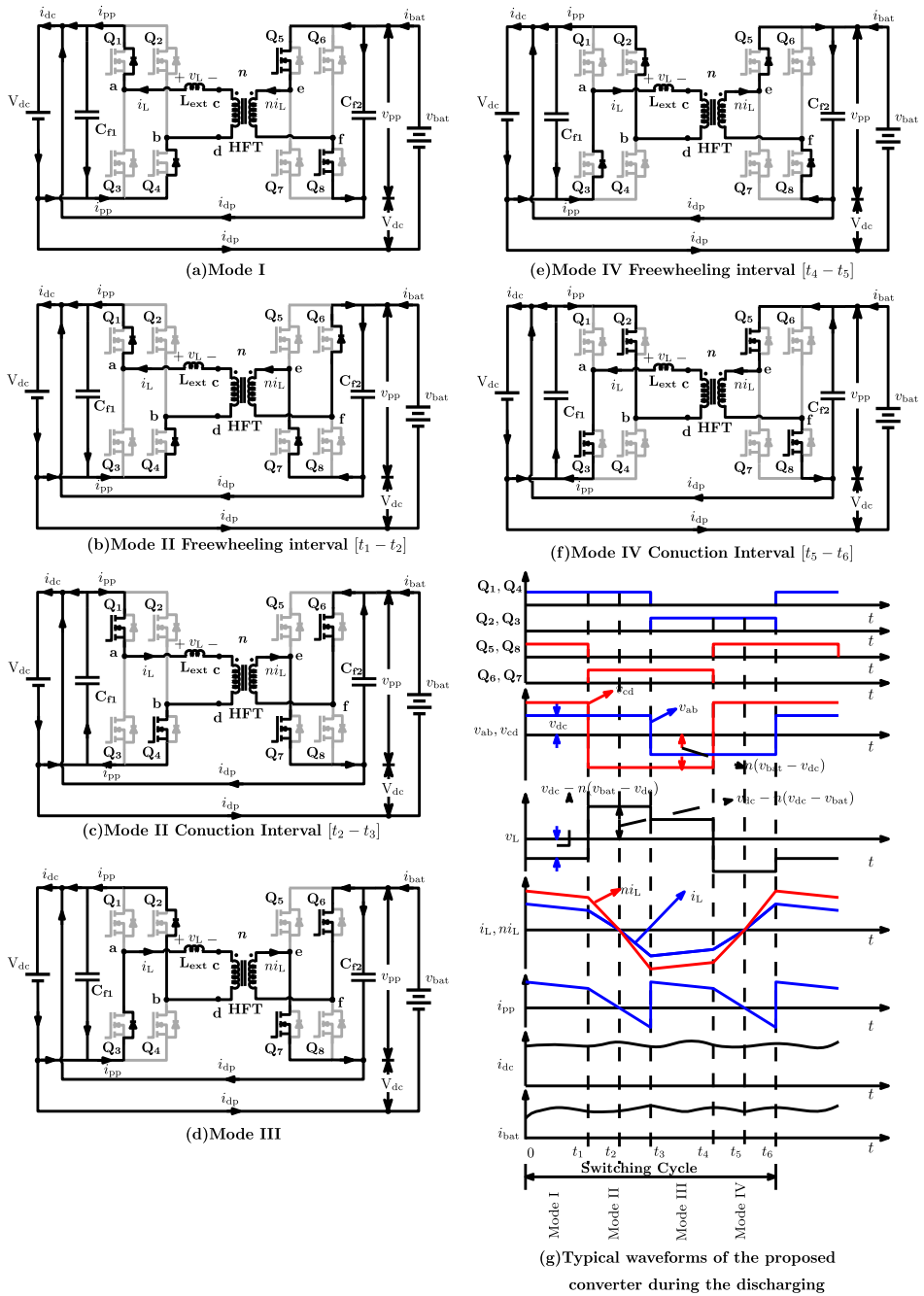


Fig. 5 – Proposed DC-DC converter modes of operation during the discharging cycle with typical waveforms.

Mode II: $t_1 < t < t_3$

This mode starts with turning OFF the Q₅-Q₈ pair and turning ON the Q₆-Q₇. The Q₁-Q₄ pair continue in the ON state from Mode I. The current ni_L was flowing through Q₅-Q₈ in the previous mode. On turning ON the Q₆ -Q₇, the current ni_L starts freewheeling through the body diodes of Q₆ and Q₇ until the current reaches zero, as shown in Fig. 5g. After the freewheeling action, the Q₆-Q₇ starts conduction, and the current ni_L reverses and rises gradually, as shown in Fig. 5g. Hence, the total switching interval of this mode can be divided into two intervals, t_1 to t_2 (freewheeling interval) and t_2 to t_3 (conduction interval). The state of the switch during these intervals is shown in Figs. 5b and 5c. Equation (17) gives the slope of the ni_L current.

$$\frac{d(ni_L)}{dt} = \frac{V_{dc} - n(V_{dc} - V_{bat})}{L_{ext}}. \quad (17)$$

Mode III: $t_3 < t < t_4$

This mode starts with the turn ON of Q₂-Q₃ and the turn OFF of Q₁-Q₄. The Q₆-Q₇ pair continues to be in the ON state from Mode II. The state of the switch during this mode is shown in Fig. 5d. The switching action results in a change of the voltage across the inductor. The change in voltage results in the change of slope of the currents i_L and ni_L ; thus, the currents i_L and ni_L falls gradually in the reverse direction. However, the slope of the inductor current throughout this mode remains constant, as can be understood from (18).

$$\frac{d(ni_L)}{dt} = \frac{-V_{dc} - n(V_{dc} - V_{bat})}{L_{ext}}. \quad (18)$$

Mode IV: $t_4 < t < t_6$

This mode starts with turning OFF the Q₆-Q₇ pair and turning ON the Q₅-Q₈. The Q₂-Q₃ pair continue in the ON state from Mode III. The current ni_L was flowing through Q₆-Q₇ in the previous mode. On turning ON the Q₅-Q₈, the current ni_L starts freewheeling through the body diodes of Q₅ and Q₈ until the current reaches zero, as shown in Fig. 5g.

After the freewheeling action, the Q₅-Q₈ starts conduction, and the current ni_L reverses and rises gradually, as shown in Fig. 5g. Hence, the total switching interval of this mode can be divided into two intervals, t_4 to t_5 (freewheeling interval) and t_5 to t_6 (conduction interval). The state of the switch during these intervals is shown in Figs. 5e and 5f. Equation (19) gives the slope of the ni_L current.

$$\frac{d(ni_L)}{dt} = \frac{-V_{dc} - n(V_{bat} - V_{dc})}{L_{ext}}. \quad (19)$$

3.1.4 Steady-state power flow analysis during discharging

The power flow from the battery to the DC source during discharge is analysed for one switching cycle. The average value of the currents and voltages are considered for this analysis. The power delivered to the DC source is given by

$$P_{dc} = V_{dc} I_{dc}. \quad (20)$$

Using (5), (20) can be written as

$$P_{dc} = V_{dc} I_{dc} = V_{dc} (I_{dp} + I_{pp}). \quad (21)$$

From (21), it can be inferred that the power delivered to the DC source, P_{dc} is contributed by two paths, the component $V_{dc}I_{bat}$ is the power contributed by the direct path P_{dp} , and the component $V_{dc}I_{pp}$ is the power contributed by the partial path, P_{pp-in} . Hence, (21) can be written as

$$P_{dc} = P_{dp} + P_{pp-in}. \quad (22)$$

The partial path input power during discharging is

$$P_{pp-out} = V_{pp} I_{bat}. \quad (23)$$

During the discharging, the ratio of partial path output power and total output power is defined as the partial power-sharing ratio, and it can be expressed as

$$K_{d-ppsr} = \frac{P_{pp-in}}{P_{dc}} = \frac{I_{pp}}{I_{bat}} = 1 - \frac{I_{bat}}{I_{dc}}. \quad (24)$$

Using (12) and (23), the partial path efficiency during discharging is

$$\eta_{d-pp} = \frac{P_{pp-in}}{P_{pp-out}}. \quad (25)$$

Using (22 – 25), the discharging efficiency of the converter solved and expressed as follows as

$$\eta_{discharging} = 1 - K_{d-ppsr} (1 - \eta_{d-pp}). \quad (26)$$

From (26), it can be inferred that the partial power-sharing ratio influences the converter's efficiency during discharge.

3.2 Power flow control

The proposed DC-DC converter has the capability to transfer power in both directions through the partial and direct paths, as shown in Fig. 3. The governing equation for controlling the power flow through the partial path during charging is given by (27).

$$P_{pp-out} = \frac{V_{dc} (V_{bat} - V_{dc}) \theta (1 - \theta / \pi)}{2\pi n f_s L_{ext}}, \quad (27)$$

where the θ is the phase shift angle in radians and, n is the turn ratio of HFT, and f_s is the switching frequency in kHz.

Similarly, the governing equation for controlling the power flow through the partial path during discharge is given by (28).

$$P_{pp-in} = \frac{(V_{bat} - V_{dc})^2 \theta(1 - \theta/\pi)}{2\pi n f_s L_{ext}} \quad (28)$$

Using (8), (9) and (27), the total output power contributed by direct and partial paths during charging is given by

$$P_{bat} = V_{dc} I_{bat} + \frac{V_{dc} (V_{bat} - V_{dc}) \theta(1 - \theta/\pi)}{2\pi f_s n L_{ext}} \quad (29)$$

Similarly, from (22) and (28), the total output power contributed by direct and partial paths during discharging is given by

$$P_{dc} = V_{dc} I_{bat} + \frac{(V_{bat} - V_{dc})^2 \theta(1 - \theta/\pi)}{2\pi f_s n L_{ext}} \quad (30)$$

From (29) and (30), it is inferred that the power transferred through the direct path remains constant for a constant value of the charging/discharging current (I_{bat}). Hence, the power flow through the partial path alone is controllable in the total power transferred during charging and discharging. Moreover, the controllable quantity in power flow through the partial path is the phase shift angle (θ) within a range of $(-\pi/2, \pi/2)$. The control strategy employed for the power flow control in the partial path is represented in Fig. 6. The function of each block is discussed in the following subsections.

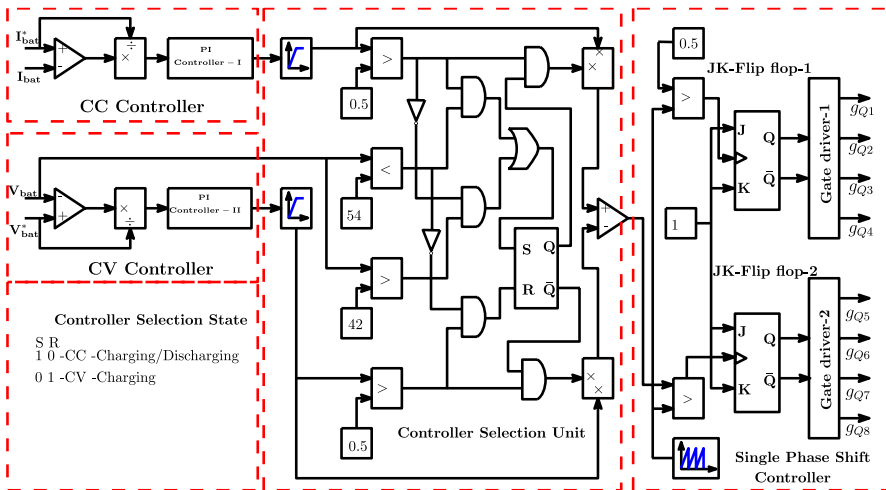


Fig. 6 – Control strategy employed for power flow control of the proposed DC-DC converter.

3.2.1 Single Phase-Shift Control strategy

Single Phase-Shift Control strategy (SPSC) is the commonly used control strategy for the configuration of the bridge network used in the proposed DC-DC converter. In SPSC, the phase shift is created by considering the source side bridge as a reference and controlling the phase shift angle (θ) on the battery side bridge. For power flow during the charging, the range of phase shift angle is $(0, \pi/2)$; during discharging, the range of phase shift angle is $(-\pi/2, 0)$.

In the SPSC used in the proposed converter, the source side bridge is driven by JK Flip Flop-1 and Gate Driver-1. Likewise, JK Flip Flop-2 and Gate Driver-2 drive the battery side bridge. Hence, the phase shift angle (θ) is created by the JK Flip Flop-2, which is governed by the control signal issued by the CSU. The functioning of the CSU is discussed in the following subsection.

3.2.2 Controller Selection Unit

The Constant Current Constant Voltage (CCCV) scheme is commonly used to charge/discharge a battery. In this scheme, the power is controlled by any one of the following methods: (i). Constant Current (CC)-Charging (ii). Constant Voltage (CV)-Charging (iii). Constant Current (CC) - Discharging. Only one of these methods can be used at any point. The CSU selects the appropriate method of charging or discharging based on the voltage at the battery's terminals, which indirectly indicates the battery's State of Charge (SoC).

The model of the battery used to estimate the terminal voltage based on the SoC is given by (31) [34]

$$V_{\text{cell}}(t) = a_0^{-a_1 \text{SoC}(t)} + a_2 + a_3^{\text{SoC}(t)} - a_4^{\text{SoC}^2(t)} + a_5^{\text{SoC}^3(t)}, \quad (31)$$

where a_0 , a_1 , a_2 , a_3 , a_4 , and a_5 are constants, $\text{SoC}(t)$ is the charge available in the battery at time t , $V_{\text{cell}}(t)$ battery single cell voltage at present $\text{SoC}(t)$.

Using (31), 380 V/18.5 Ah model considered for simulation analysis. The value of the battery's terminal voltage at 5% SoC is 355 V, and the value at 95% SoC is 410V. The CSU chooses the CC-Charging when the value of V_{bat} lies between 355V and 410V and the reference current (I_{bat}) is positive. It chooses CC-discharging when the V_{bat} is above 363 V and I_{bat} is set to negative. CV-Charging will be chosen when the value of V_{bat} is above 410V. Hence, the overall function of the CSU is to send the control signals from the suitable controller based on the reference currents and the battery terminal voltage so that the SPSC generates appropriate phase-shifted gate signals to vary the phase shift angle (θ).

3.2.3 CC and CV Controller

The CC and CV controller are commonly used controllers for charging the battery. They are fed by the voltage (V_{bat}) and current (I_{bat}) at the terminals of the battery fetched through voltage and current sensors, as shown in Fig. 2. Both the controllers compare the respective quantities with the reference values and feed

the error to their PI controllers as shown in Fig. 6. The PI controllers generate the control signals which will be routed to the SPSC by the CSU depending on the operating scenario.

4 Results and Discussions

4.1 Simulation results

The proposed DC-DC converter with the control strategy shown in Fig. 2 is simulated in MATLAB/Simulink. The power rating of the DC-DC converter is chosen as 7.8 kW. The other parameters considered are mentioned in **Table 1**. The proposed converter is simulated for the following case studies of charging and discharging, and the performance is analysed.

Table 1
Simulation Parameters.

SIMULATION PARAMETERS	VALUE
Input Voltage (V_{dc})	240 V
External Inductor (L_{ext})	36 μ H
HFT Capacity (VA)	3000 VA
HFT Turns ratio (n)	0.83
Switching frequency (f_s)	50 kHz
Filter Capacitances (C_{f1}, C_{f2})	650 μ F, 450 μ F
Battery capacity	380 V, 18.5 Ah
Charging Current (I_{bat})	18.5 A
Discharging Current (I_{bat})	18.5A
PI Controller-I	$k_{pc}=2.4, k_{ic}=12.8$
PI Controller-II	$k_{pv}=5.4, k_{iv}=27$

4.1.1 Steady state simulation: CC-CV Charging

In this case study, the proposed DC-DC converter's performance is analysed during the charging cycle. The initial SoC of the battery is considered as 5%, and the reference values are set as $I_{bat}^*=18.5$ A and $V_{bat}^*=355$ V. The system is simulated for a duration until the SoC reaches 95%. The variations in various quantities were plotted and shown in Fig. 7. Overall, the charging mode was in CC- Charging until the SoC reached 95% and changed to CV-Charging for SoC above 95%.

From Fig. 7, the following points can be inferred regarding the performance of the converter:

- The voltage of the battery terminals rises gradually during the charging cycle. The voltage provided by the direct path remains constant, which is the voltage of the DC source. However, the voltage provided by the partial path gradually increases until the SoC reaches 95%. Hence, the voltage variation is attributed to the controllable partial path power.

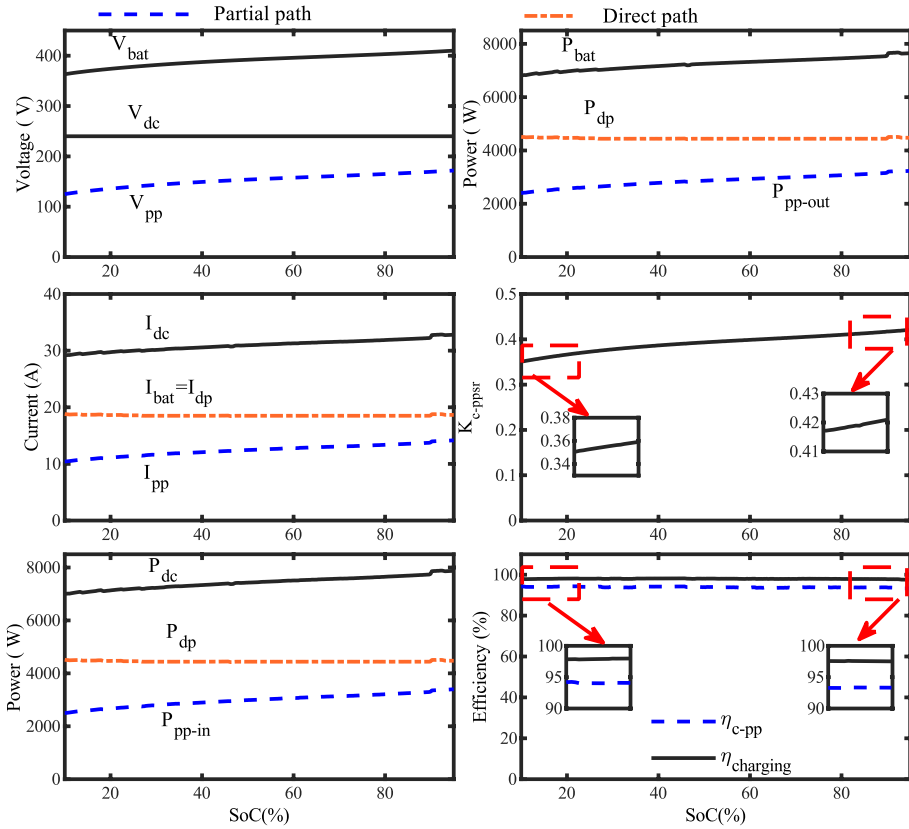


Fig. 7 – Performance of the proposed DC-DC Converter during the Charging Cycle.

- During the charging cycle, until the SoC reaches 95%, the current that enters the source side bridge (I_{pp}) and the source current (I_{dc}) is observed to rise gradually, whereas the current (I_{dp}) flowing in the direct path is constant. Interestingly, the current flowing to the battery is the current from the direct path, i.e., $I_{bat} = I_{dp}$.
- The proposed converter generally delivers a voltage 270-420V range. The nominal voltage of 380V, 18.5Ah battery completes the charging cycle, and the converter delivers 356-420V at 18.5A charging current. During this charging cycle, the partial path only supports and regulates the voltage V_{pp} , and it varies from 120 to 180V. The rest of voltage of fixed $V_{dc}=240V$ is supported by the direct path.
- The power flow to the battery contributed by the direct path (P_{dp}) is constant and the one contributed by the partial path (P_{pp}) rises gradually until the SoC reaches 95%. Also, the partial power-sharing ratio (K_{c-ppsr}) rises gradually

and reaches a maximum value of 0.42. In other words, the partial power path contributes only a maximum of 42% of the total power delivered to the battery and the direct power path contributes a minimum of 58%. Hence, the lossy partial path contributes less than 50% of the total power, so the losses are minimised.

- The converter's efficiency during the charging cycle stays within 97.85%. The significant contribution to achieving the high-efficiency transfer is attributed to the lossless power transfer through the direct path that contributes at least 58% of the total power delivered to the battery at any time.

From the analysis of the performance of the proposed converter during the charging cycle, it can be observed that the power flow through the direct path is constant throughout the charging cycle. In contrast, the power flow through the partial path is variable and controllable. The high efficiency is significantly attributed to the higher share of power flow through the lossless direct path.

4.1.2 Steady-state simulation: CC-Discharging

This case study analyses the proposed DC-DC converter's performance during the discharging cycle. The initial SoC of the battery is 98%, and the reference values are set as $I_{\text{bat}}^* = -18.5$ A and $V_{\text{bat}} = 412$ V. Setting I_{bat}^* negative means that the direction of the current is in reverse in the discharge cycle. Hence, the current flow from the battery to the source is considered positive during the discharging cycle. The system is simulated for a duration until the SoC reaches 10%. The variations in various quantities were plotted and shown in Fig. 8. The battery discharged in CC-discharging mode and ended with SoC falling to 10%.

From Fig. 8, the following points can be inferred regarding the performance of the converter:

- The DC source voltage, the partial path, and the direct path voltage on the source side remain constant throughout the discharge cycle. However, the voltage at battery terminals falls gradually during the discharging cycle until the SoC falls to 10%. Now, as the voltage of the direct path is held constant by the DC source, the variation in the battery terminal voltage will be taken up by the partial path voltage across the bridge on the battery side (V_{pp}).
- The current delivered to the DC source from the battery is contributed by the direct path current (I_{dp}) and partial path current (I_{pp}). The direct path current is constant and equal to the current flowing out from the battery terminals, i.e., ($I_{\text{dp}} = I_{\text{bat}}$). The current flow from the partial path (I_{pp}) gradually falls, with the SoC falling up to 10%.
- The power flow to the DC source contributed by the direct path (P_{dp}) is constant, and the one contributed by the partial path ($P_{\text{pp-in}}$) falls gradually until the SoC reaches 10%. Also, the partial power-sharing ratio $K_{\text{d-ppsr}}$ falls

gradually from a maximum value of 0.40. At the end of battery discharge, K_{d-ppsr} is 0.34. In other words, the partial power path contributes only a maximum of 40% of the total power delivered to the DC source from the battery, and the direct power path contributes a minimum of 60%. Hence, the lossy partial path contributes less than 40% of the total power, so the losses are minimised.

The converter's efficiency during the discharging cycle stays within the 95% to 95.6% range. The significant contribution to achieving the high-efficiency transfer is attributed to the lossless power transfer through the direct path that contributes at least 60% of the total power delivered to the DC source from the battery at any time.

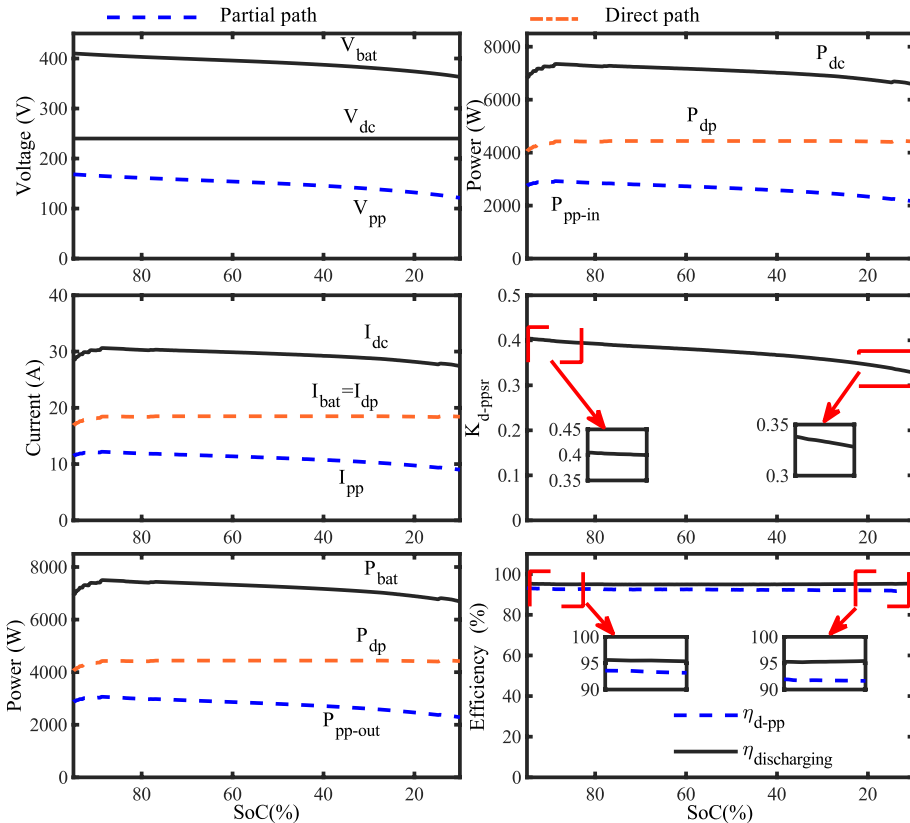


Fig. 8 – Performance of the proposed DC-DC Converter during the Discharging Cycle.

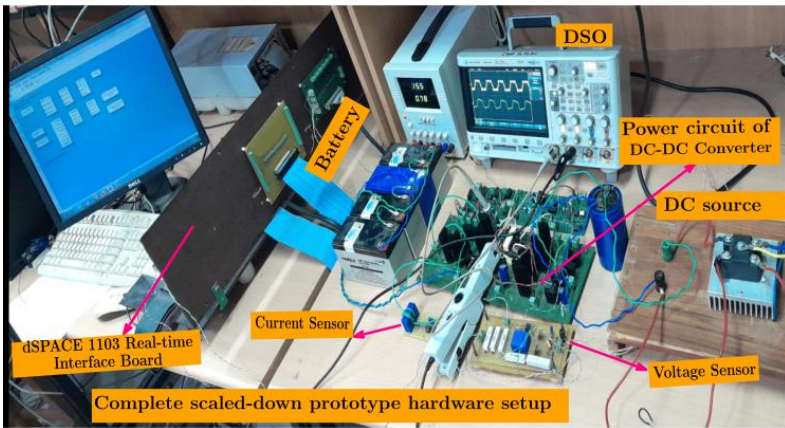
From the analysis of the performance of the proposed converter during the discharging cycle, it can be observed that the power flow through the direct path is constant throughout the discharging cycle. In contrast, the power flow through

the partial path is variable and less than 40% of the total delivered power to the source in the complete discharging cycle. The high efficiency is significantly attributed to the higher share of power flow through the lossless direct path.

In the next section, a 600 W power rating of the proposed DC-DC converter is implemented in a hardware scaled-down prototype, and its performance is validated.

4.2 Experimental results

A 600 W down-scaled prototype of the proposed DC-DC converter is developed, and its performance is analysed. The developed down-scaled prototype hardware setup of the proposed DC-DC converter and its DC-DC converter layout design are shown in Fig. 9.



(a)



(b)

Fig. 9 – Experimental set up of the proposed DC-DC converter: (a) Complete prototype hardware setup; (b) DC-DC converter layout.

The complete design parameters considered for the development of the hardware prototype are given in **Table 2**. The instantaneous voltage and current at the battery terminals are sensed by the voltage sensor (LV25-P) and current sensor (LA-55-P), respectively. The scaled-down values received from these sensors are fed to the Analog to Digital Converter (ADC) port of the dSPACE DS1103 Real-Time Interface (RTI) board. The dSPACE implements the CC and CV controllers along with the CSU shown in Fig. 6.

The dSPACE generates a set of PWM signals at twice the switching frequency. One PWM signal has a fixed duty ratio of 0.5, and the other PWM signal has a variable duty ratio decided by the operating mode (i.e., CC-Charging, CV-Charging and CC-Discharging).

Table 2
Experimental Parameters.

DESIGN ASPECTS	PARAMETERS / MATERIAL PARTS	VALUE
Converter Design	Input Voltage (V_{dc})	30 V
	Maximum power ratings	600 W
	Switching frequency(f_s)	50 kHz
	Power semiconductor (MOSFET)	IRF640N
HFT design	HFT Capacity (VA)	350 VA
	Turns ratio (n)	0.89
	E Core dimension	N87 Material, E42/21/20
	Coil former	GFR Polyterephthalate
	Enameled copper wire	26 AWG
	Filter Capacitance (C_{f1}, C_{f2})	100V, 150 μ F, 63V, 100 μ F
Battery Specification	Voltage	48V
	Capacity	12.5 Ah
	Type	Lead Acid
Controllers Specification	PI Controller-I	$k_{pe}=1.8, k_{ie}=5$
	PI Controller-II	$k_{pv}=2.4, k_{iv}=8$
SPSC design specification	Buffer IC	SN7407
	JK flip flop	CD74HC73E
	Optocoupler IC	HCPL 3120

The PWM signals generated by the dSPACE are fed as input to the JK-flip flops (negative edge triggered) on the SPSC board. The JK-flip flop-1 generates two signals at switching frequency and feeds them to the Gate driver-1, which in turn generates two sets of PWMs for the source side MOSFETs. The JK-flip flop-2 also generates two signals at switching frequency and feeds them to the Gate driver-2, which in turn generates two sets of PWMs for the battery side MOSFETs. The negative edge triggering employed by the JK-flip flops ensures the required phase shift between the source and battery side bridges.

The steady-state and dynamic performance of the developed hardware prototype converter are analysed in the following subsections.

4.2.1 Steady-state response of the developed hardware prototype DC-DC converter

The steady-state voltages and currents for a set reference of $V_{\text{bat}}^* = 48 \text{ V}$ and $I_{\text{bat}}^* = 4 \text{ A}$ during the charging cycle is shown in Fig. 10a. Similarly, steady-state voltages and currents for a set reference of $I_{\text{bat}}^* = -6 \text{ A}$ during the discharging cycle is shown in Fig. 10b.

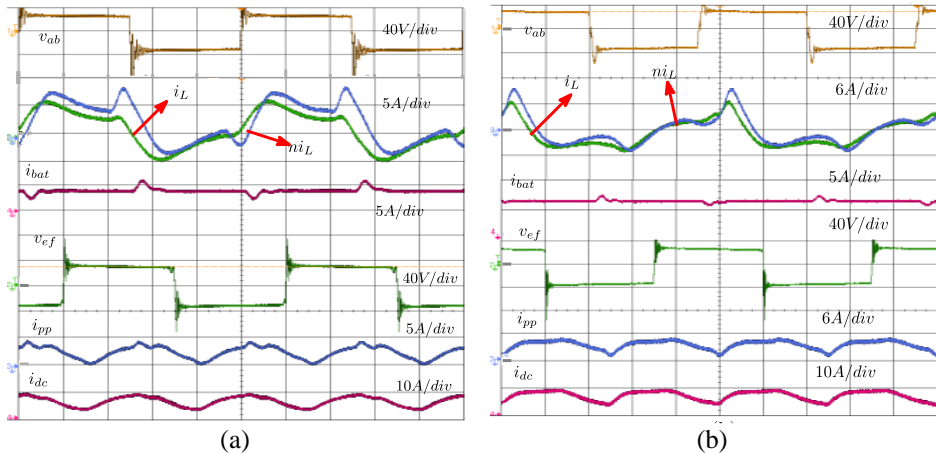


Fig. 10 – Experimental Results during: (a) Charging; (b) Discharging.

Further, the performance of the proposed converter for various reference values of charging and discharging currents is analysed. For different values of the reference current I_{bat} chosen, the overall efficiency (η_{charging} , and $\eta_{\text{discharging}}$), the efficiency of the partial path ($\eta_{\text{c-pp}}$, $\eta_{\text{d-pp}}$) and the partial path power-sharing ratio ($K_{\text{c-ppsr}}$ and $K_{\text{d-ppsr}}$) values obtained through experimentally, and their results are presented graphically, as shown in Fig. 11.

From the results presented in Fig. 11a, it can be observed that the overall practical system efficiency during charging is in the range of 93.5% to 97%. Also, results show that the partial power-sharing ratio, $K_{\text{c-ppsr}}$, always stayed below 0.45.

Hence, a minimum of 55% of the power flow to the battery is always contributed by the lossless direct power path. So, the proposed converter has proved to be highly efficient experimentally for a wide range of operating conditions during charging.

From the results presented in Fig. 11b, it can be observed that the overall practical system efficiency during discharge is in the range of 95% to 97%. Also, the partial power sharing ratio, $K_{\text{d-ppsr}}$ stayed below 0.4 always. Hence, the lossless direct path always contributes a minimum of 60% of the power flow to the DC source from the battery. So, the proposed converter has proved experimentally efficient for various operating conditions during discharging.

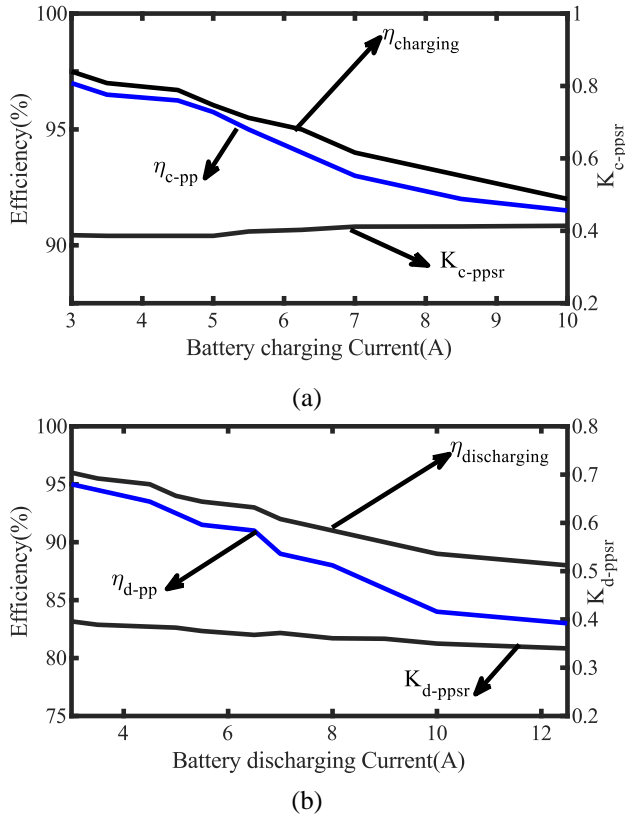


Fig. 11 – Steady-state performance of the proposed converter for various set values of reference current (I_{bat}^*) during: (a) Charging; (b) Discharging.

From the experimental steady-state analysis of the performance of the proposed DC-DC converter, it is proved that the proposed converter is highly efficient during both the charging and discharging, with a higher share of power flow through the lossless direct path.

4.2.2 Experimental response for Step Change in battery reference current during Charging and Discharging

The scaled-down hardware setup of the proposed DC-DC converter has been analysed for the step change in the battery reference current (I_{bat}^*) during charging and discharging. The initial I_{bat}^* was 6.25 A during charging, and a step change to 4 A is given at t_{1cc} . The values of voltages and currents reached a steady state after a short transient period, as shown in Fig. 12a. Similarly, the initial I_{bat}^* was 9 A during discharge, and a step change to 6 A is given at t_{1dc} . The values of voltages and currents reached a steady state after a short transient period, as shown in Fig. 12b. From Figs. 12a and 12b, it can be inferred that the proposed

converter can adapt to the changing reference currents and provide a stable operation.

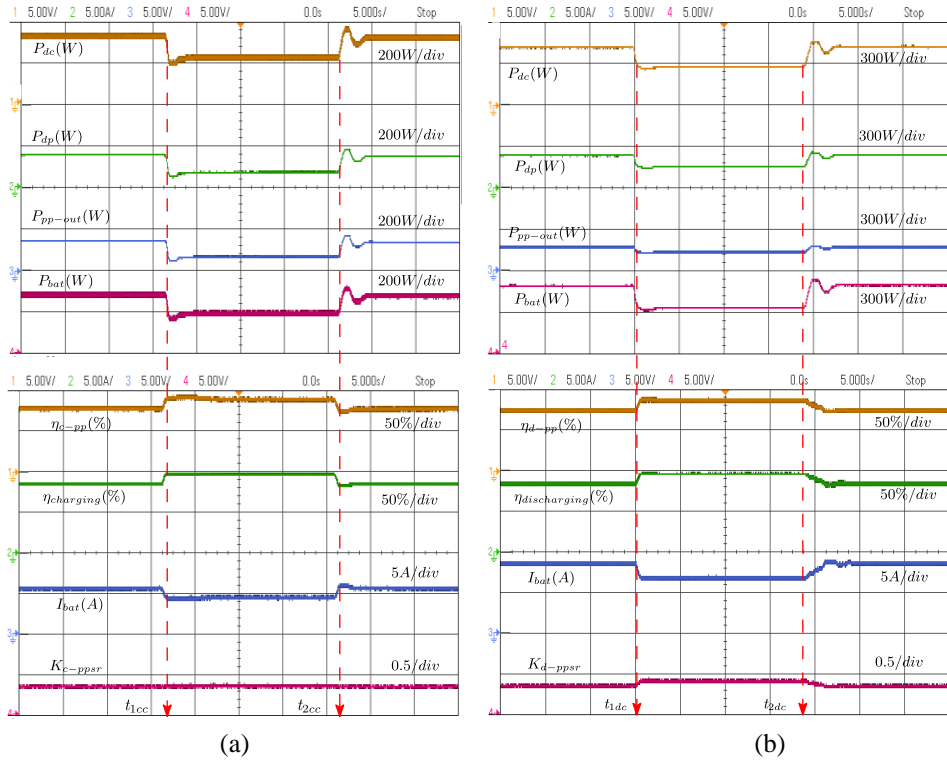


Fig. 12 – Step changes response of the proposed DC-DC Converter during: (a) Charging; (b) Discharging.

The proposed DC-DC converter has many advantages, such as high-power density, wide operating voltage range (270 – 420V), higher efficiency, and bidirectional power transfer capability. The voltage range supports the charging of EV batteries at a maximum power of 7.8 kW. The power transfer feature offers the design of compact and high-efficiency bidirectional OBC for upcoming EVs.

A possible concern about the proposed converter would be the absence of galvanic isolation between the battery and the DC-DC converter. However, as per the safety standards SAEJ1772 and AIS-138, galvanic isolation is not mandatory for OBC [31 – 33]. Safety is ensured since the battery terminals always float on the vehicle's body. Furthermore, SAEJ1772 standard OBC has five terminals, i.e., phase, neutral, Connection Switch (CS), Protection Earth (PE), and Control Pilot (CP) terminals [35]. The PE terminal of the OBC will take care of the protection from electric shock. Hence, the non-isolation of the DC-DC stage will not be problematic for an OBC that complies with the SAEJ1772 standard.

5 Comparison with Other Similar Work

From an On-Board EV point of view, the DC-DC converter should have the least number of components to reduce the charger's overall weight, which can influence the vehicle's kWh/mile.

Also, it is expected to deliver power at high efficiency, as is the case with any power conversion equipment. In addition, the DC-DC converter should have bidirectional power flow capability if the EV desires to have V2G and V2V power transfer capability. In this regard, the performance of the proposed DC-DC converter is compared to other recent works and presented in **Table 3**.

Table 3
Comparison with Similar works.

Ref.	[6]	[11]	[12]	[13]	[16]	[17]	[18]	[23]	Proposed converter
Semiconductor Devices (Nos)	14	12	10	14	14	12	12	16	8
Inductor (Nos)	3	2	2	3	3	2	1	-	1
Capacitors (Nos)	5	2	4	3	8	2	2	4	2
Transformer (Nos)	2	1	1	1	2	1	2	2	1
Total Components	24	17	17	21	27	17	17	22	12
Switching frequency (kHz)	40	-	150-450	200	200	200	110	300	50
Fixed Duty ratio	No	Yes	No	Yes	No	No	No	No	Yes
Isolation	Yes	No	Yes	Yes	Yes	Yes	Yes	Yes	No
Input Voltage (V)	400	120-375	370-410	100-420	700	390	400	400	240
Output Voltage (V)	250-450	270-430	36-72	120-375	50-650	250-420	320-420	250-450	270-420
Power Rating (kW)	3.7	3.7	3.7	1	20	1	3.3	6.6	7.8
Current ratings (A)	8.5	13.8	50	2.5	30	2.5	8.25	14.6	18.5
Bidirectional power transfer	No	No	No	Yes	No	No	No	Yes	Yes
Direct power transfer	No	Yes							
Charging cycle Efficiency (%)	98.3	97.6	96	93.5	97	95.1	96.3	96	97.8
Discharging cycle Efficiency (%)	NA	-	95.6						
NA-Not Applicable, as those configurations do not support bidirectional feature									

From the detailed comparison presented in **Table 3**, it can be inferred that the proposed DC-DC converter uses the least number of components and can provide an efficient power transfer compared to the existing works. Using fewer components reduces cost, so an efficient charger at a lower price is possible. Also, the proposed converter has a bidirectional power flow feature. In contrast, the converters in the other works do not have a bidirectional feature, which plays a vital role in incorporating the V2G and V2V power transfer features in EVs. Hence, it has been shown that the proposed DC-DC converter will be an efficient and compact solution for On-Board EV applications with V2G and V2V power transfer capabilities.

6 Conclusion

This paper proposes a novel bidirectional DC-DC converter with partial and direct power flow paths for an On-Board Charger for EVs. The performance is validated in simulation for various operating scenarios and is an efficient solution. A prototype DC-DC converter using the proposed topology with a rating of 600W is developed to validate experimentally. The prototype's performance is tested for steady-state and step change conditions and found to adapt to step changes and provide a stable operation. The noteworthy observations from the results can be stated as follows:

- In the proposed DC-DC converter, only 35-42% of the power is transferred through the partial path, and a significant share of 58-65% is transmitted through a lossless direct path during the charging/discharging cycle. Hence, an efficiency of 95-95.6% during the charging cycle and 97.85% during the discharging cycle has been achieved.
- The reduced power flow through the partial path significantly reduced the rating of semiconductor switches and the size of the passive components and HFT.

Based on the comparison with similar works, it has been shown that the proposed DC-DC converter uses the least number of components, has bidirectional power flow capability, and can achieve high efficiency. The highly efficient power processing capability at a reduced size can significantly reduce the overall costs of chargers and electric vehicles. Hence, the proposed DC-DC converter for an On-Board Charger provides an efficient and compact solution for the modern electric vehicle and makes it capable of V2G and V2V power transfer.

7 References

- [1] D. K. Wui Lo, F. Juwono, W. K. Wong, I. M. Chew: A Study on Transmission Coil Parameters of Wireless Power Transfer for Electric Vehicles, *Serbian Journal of Electrical Engineering*, Vol. 19, No. 2, June 2022, pp. 129 – 145.

- [2] I.- O. Lee: Hybrid DC–DC Converter with Phase-Shift or Frequency Modulation for NEV Battery Charger, *IEEE Transactions on Industrial Electronics*, Vol. 63, No. 2, February 2016, pp. 884 – 893.
- [3] I. Aretxabaleta, I. Martinez De Alegria, J. Andreu, I. Kortabarria, E. Robles: High-Voltage Stations for Electric Vehicle Fast-Charging: Trends, Standards, Charging Modes and Comparison of Unity Power-Factor Rectifiers, *IEEE Access*, Vol. 9, June 2021, pp. 102177–102194.
- [4] H. Tu, H. Feng, S. Srdic, S. Lukic: Extreme Fast Charging of Electric Vehicles: A Technology Overview, *IEEE Transactions on Transportation Electrification*, Vol. 5, No. 4, December 2019, pp. 861 – 878.
- [5] J. Rojas, H. Renaudineau, S. Kouro, S. Rivera: Partial Power DC-DC Converter for Electric Vehicle Fast Charging Stations, *Proceedings of the 43rd Annual Conference of the IEEE Industrial Electronics Society (IECON)*, Beijing, China, October 2017, pp. 5274 – 5279.
- [6] C. Liu, B. Gu, J.- S. Lai, M. Wang, Y. Ji, G. Cai, Z. Zhao, C.- L. Chen, C. Zheng, P. Sun: High-Efficiency Hybrid Full-Bridge–Half-Bridge Converter with Shared ZVS Lagging Leg and Dual Outputs in Series, *IEEE Transactions on Power Electronics*, Vol. 28, No. 2, February 2013, pp. 849 – 861.
- [7] I. Hammoud, N. Bauer, I. Kalfass, R. Kennel: Optimized Capacitive Active Ripple Compensation Topology for a 3.7 kW Single-Phase High Power Density On-Board Charger of Electric Vehicles, *Electrical Engineering*, Vol. 101, No. 3, September 2019, pp. 685 – 697.
- [8] L. Xue, Z. Shen, D. Boroyevich, P. Mattavelli, D. Diaz: Dual Active Bridge-Based Battery Charger for Plug-in Hybrid Electric Vehicle with Charging Current Containing Low Frequency Ripple, *IEEE Transactions on Power Electronics*, Vol. 30, No. 12, December 2015, pp. 7299 – 7307.
- [9] M. Brenna, F. Foidadelli, C. Leone, M. Longo: Electric Vehicles Charging Technology Review and Optimal Size Estimation, *Journal of Electrical Engineering & Technology*, Vol. 15, No. 6, November 2020, pp. 2539 – 2552.
- [10] R. Maurya, S. R. Arya, R. K. Saini, J. Gupta: On-Board Power Quality Charger for Electric Vehicles with Minimized Switching Stresses, *Electrical Engineering*, Vol. 104, No. 3, June 2022, pp. 1667 – 1680.
- [11] C.- Y. Oh, D.- H. Kim, D.- G. Woo, W.- Y. Sung, Y.- S. Kim, B.- K. Lee: A High-Efficient Nonisolated Single-Stage On-Board Battery Charger for Electric Vehicles, *IEEE Transactions on Power Electronics*, Vol. 28, No. 12, December 2013, pp. 5746 – 5757.
- [12] F. Musavi, M. Craciun, D. S. Gautam, W. Eberle: Control Strategies for Wide Output Voltage Range LLC Resonant DC–DC Converters in Battery Chargers, *IEEE Transactions on Vehicular Technology*, Vol. 63, No. 3, March 2014, pp. 1117 – 1125.
- [13] C. Shi, H. Wang, S. Dusmez, A. Khaligh: A SiC-Based High-Efficiency Isolated Onboard PEV Charger with Ultrawide DC-Link Voltage Range, *IEEE Transactions on Industry Applications*, Vol. 53, No. 1, January-February 2017, pp. 501 – 511.
- [14] D. Zinchenko, A. Blinov, A. Chub, D. Vinnikov, I. Verbytskyi, S. Bayhan: High-Efficiency Single-Stage On-Board Charger for Electrical Vehicles, *IEEE Transactions on Vehicular Technology*, Vol. 70, No. 12, December 2021, pp. 12581 – 12592.
- [15] M. Khalid, F. Ahmad, B. K. Panigrahi, L. Al-Fagih: A Comprehensive Review on Advanced Charging Topologies and Methodologies for Electric Vehicle Battery, *Journal of Energy Storage*, Vol. 53, September 2022, p. 105084.

- [30] M. S. Bhaskar, V. K. Ramachandaramurthy, S. Padmanaban, F. Blaabjerg, D. M. Ionel, M. Mitolo, D. Almakles: Survey of DC-DC Non-Isolated Topologies for Unidirectional Power Flow in Fuel Cell Vehicles, *IEEE Access*, Vol. 8, September 2020, pp. 178130 – 178166.
 - [31] D.- H. Kim, B.- K. Lee: Asymmetric Control Algorithm for Increasing Efficiency of Non-Isolated On-Board Battery Chargers with a Single Controller, *IEEE Transactions on Vehicular Technology*, Vol. 66, No. 8, August 2017, pp. 6693 – 6706.
 - [32] A. V. J. S. Praneeth, S. S. Williamson: Modeling, Design, Analysis, and Control of a Nonisolated Universal On-Board Battery Charger for Electric Transportation, *IEEE Transactions on Transportation Electrification*, Vol. 5, No. 4, December 2019, pp. 912 – 924.
 - [33] H. Karneddi, D. Ronanki: Universal Bridgeless Nonisolated Battery Charger with Wide-Output Voltage Range, *IEEE Transactions on Power Electronics*, Vol. 38, No. 3, March 2023, pp. 2816 – 2820.
 - [34] T. Kim, W. Qiao: A Hybrid Battery Model Capable of Capturing Dynamic Circuit Characteristics and Nonlinear Capacity Effects, *IEEE Transactions on Energy Conversion*, Vol. 26, No. 4, December 2011, pp. 1172 – 1180.
- A. Khaligh, M. D'Antonio: Global Trends in High-Power On-Board Chargers for Electric Vehicles, *IEEE Transactions on Vehicular Technology*, Vol. 68, No. 4, April 2019, pp. 3306 – 3324.